ACS OMEGA

http://pubs.acs.org/journal/acsodf

Article

# Disulfide Bridged Nanoparticles of Thiolated Sodium Alginate and Eudragit RS100 for Oral Delivery of Paclitaxel: *In Vitro* and *In Vivo* Evaluation

Hafiz Muhammad Bilal Khalid, Akhtar Rasul,* Shahid Shah,* Ghulam Abbas, and Abid Mahmood

Cite This: *ACS Omega* 2023, 8, 9662−9672

Read Online

ACCESS | Metrics & More | Article Recommendations | Supporting Information

**ABSTRACT:** Most biopharmaceutics classification system (BCS) class IV drugs have limited oral bioavailability due to poor solubility and poorer permeability. This work aims to investigate the possibility of utilizing disulfide bridged nanoparticles to improve BCS IV drug solubility and oral absorption. Disulfide bridged nanoparticles were made using thiolated sodium alginate (TSA) and thiolated eudragit RS100 (TERS100). This study used paclitaxel (PTL) as a model drug to create PTL-loaded nanoparticles using the air oxidation approach. PTL-loaded nanoparticles boosted the solubility of PTL by over 11 times (~59 μg/mL). The nanoparticles had particle sizes of 103 nm, polydispersity indices of 0.034, and zeta potentials of −21 mV, respectively. Nanoparticles demonstrated 75.34% and 89.18% entrapment and loading efficiency of PTL, respectively. The PTL release data from nanoparticles had good sustained release properties. The effective permeability of PTL from nanoparticles was 2.19-fold higher than that of pure PTL suspension. The relative bioavailability of PTL with disulfide bridged nanoparticles was 237.11%, which was much higher than that of PTL suspension, according to the pharmacokinetic data. These results show that disulfide bridged nanoparticles have a wide range of clinical applications.

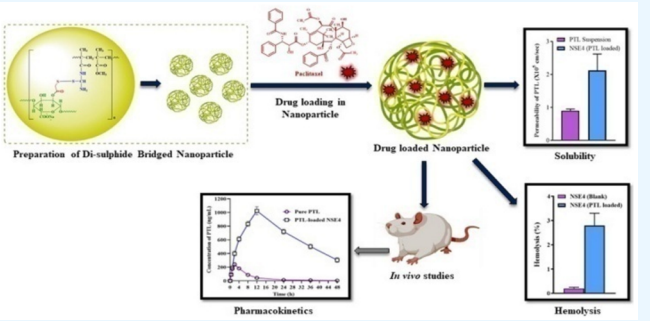


## 1. INTRODUCTION

Numerous researchers have recently expressed concern in the creation and improvement of colon-targeted drug delivery systems, which provide possible treatments for a variety of illnesses, like colorectal cancer.[1] Colon medication delivery systems reduce any adverse effects, allowing for successful drug administration to the area affected by colon disease. Additionally, this method offers a lengthy retention period for colon drug localization, which will enhance absorption of drug into the systemic circulation.[2] The oral route is used for colon drug delivery since it is flexible and improves patient compliance. It is also the most convenient administration route.[3]

Natural polysaccharides like sodium alginate (SA) have strong bioadhesion, biocompatibility, and swelling properties. Drugs loaded with polysaccharides have a delayed release and are difficult to inactivate.[4] Consequently, polysaccharides are used as a drug carrier in the majority of bioadhesive colon focused drug delivery systems. In contrast to the stomach and small intestine, which are acidic environments, the colon is alkaline, and SA dissolves there, where it binds to the colon walls. As a result, alginate is frequently employed as a medication delivery system for colon-specific drugs.[5] Over the past ten years, the importance of ERS100, a synthetic polymer with a pH verge of more than 7, has grown in the field of medicinal formulations.[6] Some of the features that make ERS100 a reliable choice for treating colorectal malignancies are gut targeting and value in sustained drug release. We have the possibility to improve the efficacy of drug therapy and transition to an oral route of drug administration by combining ERS100 with SA nanoparticulate systems.

Numerous populations of microorganisms can create reducing environments for various compounds, including azo, nitro, and disulfide bonds, in the human colon. Due to their stability in extra-cellular fluids as opposed to intracellular fluids with glutathione (GSH), which decreases the environment for disulfide couplings, polymers with disulfide bonds are extensively studied. The concentration of GSH is 7−10 times higher in cancer cells than in healthy cells. Therefore, adding disulfide cross-links to polymers can be a workable alternative technique in research looking at drug delivery for colon cancer. However, due to the generally low reductive environment, disulfide bond low reduction processes can still take place in normal cells. The best way to overcome this

Received: January 19, 2023
Accepted: February 22, 2023
Published: March 3, 2023

ACS Publications

© 2023 The Authors. Published by American Chemical Society



https://doi.org/10.1021/acsomega.3c00400
*ACS Omega* 2023, 8, 9662−9672

difficulty is to utilize cross-linked nanoparticles with disulfide bonds as the core, which will prevent early drug release and toxicity in normal cells.[5]

Paclitaxel (PTL), a natural anticancer chemotherapeutic agent, has limited solubility and permeability that compromise its pharmacological benefit.[7] The nonpolar, lipophilic, and nonionizable nature of PTL negatively impacts its solubility. PTL is within the biopharmaceutical classification system (BCS) IV drug, which is the most difficult to administer orally. By emphasizing delivery of medications to the target locations to reduce accumulation of drug at nonspecific sites, nanotechnology has also emerged as a viable method for enhancing treatment outcomes. To get beyond the current constraints in the colon-targeted medication delivery system, new systems and technologies need to be created and investigated. Modifying the properties of nanoparticles can increase the efficacy of drug carriers and reduce side effects.[2]

The purpose of this study is to prepare SA-ERS100 nanoparticles by disulfide-bond formation TSA and TERS100 for the treatment of colorectal cancer. The technique has an advantage over the traditional ionic gelation process since it produces smaller particles with a narrower size distribution. Scanner electron microscopy (SEM), differential scanning calorimetry (DSC), Fourier transform infrared (FTIR) spectroscopy, thermogravimetric analysis (TGA), and other methods are used to analyze the physiochemical properties of nanoparticles. On the human Caco-2 cell line, a cytotoxicity investigation was evaluated. The model drug used to examine drug permeability, pharmacokinetics, and release characteristics is PTL.

## 2. MATERIALS AND METHODS

**2.1. Materials.** Thiourea and thioglycolic acid was acquired from Sigma-Aldrich Gmbh Germany. Sodium alginate (SA), acetonitrile, ethanol, and methanol were acquired from Merck, Germany. Eudragit RS100 (ERS100) and 5,5-dithiobis (2-nitrobenzoic acid) (DTNB) were bought from BDH Wharf-Road, London. Monopotassium phosphate was bought from Dae-Jung, Korea. Paclitaxel (PTL) was gifted by a Pharmasol company.

**2.2. Thiolation of Sodium Alginate (SA).** An esterification method was used to prepare thiolated sodium alginate (TSA) with the help of TGA. For sample preparation, first we heat the water (20 mL) at 80 °C and mix it with 1 g of SA and make it a homogenized solution with continuous stirring. Then add TGA (98%) with the previously prepared SA but with the different ratios, i.e., 1:1, 1:1.25, 1:1.50, 1:1.75, and 1:2 of TGA and SA. After that this solution was put on water bath at 80 °C for 3 h and add already prepared 7 N HCl (1 mL) solution was added in it drop by drop with the span of 10 min. 30 mL of methanol was used to get precipitation of TSA and to eliminate the free unbound thiol completely washed the solution with pure methanol twice and put it in at 25 °C to dry for 24 h. The mathematical equation (eq 1) was utilized to calculate the percentage yield.[8]

$$\text{Percentage yield} = \frac{\text{Practical yield}}{\text{Theoratical yield}} \times 100 \quad (1)$$

**2.3. Thiolation of Eudragit RS100 (ERS100).** First, we prepared 50 mL of a 1% solution of ERS100 in phosphate buffer with a pH of 7.4 and 50 mL of a thiourea (0.1M) solution in distilled water. The mixture was then placed for 2 min in an oven at 40 °C. The mixture was taken out of the oven, hydrolyzed with 20 mL of NaOH solution, and then returned to the oven for another 1.5 min at 40 °C. After being removed from the oven and given time to cool, the mixture was neutralized by adding 20 mL of HCl (0.1M) solution. White precipitates were produced after the addition of ethanol (10 mL), separated, washed three times with acetone, and dried at 45 °C.[9]

**2.4. Preparation of Nanoparticles.** The preparation of nanoparticles involved the air oxidation process. When compared to the ionic gelation process, the air oxidation method produces nanoparticles with smaller particle sizes. The method described by Iqbal et al. was slightly modified in order to synthesize the nanoparticles.[9] By varying the ratios of TSA and TERS100, the five different nanoparticle formulations were made (NSE1 to NSE5) as shown in Table 1. TERS100 was dissolved in phosphate buffer with a pH of 7.4, and TSA was dissolved in distilled water in a specific amount before being mixed. Place this mixture on a magnetic stirrer for 12 h. After 12 h, centrifuge the excess reactants for 15 min at 15,000 rpm to remove them. With deionized water, the pellets were centrifuged three times, lyophilized, and kept at 4 °C.

**Table 1. Composition of Prepared Disulfide Bridged Nanoparticles with Different Ratios of TSA and TERS100**

| code | TSA | TERS100 |
|---|---|---|
| NSE1 | 1 | 2 |
| NSE2 | 2 | 1 |
| NSE3 | 1 | 3 |
| NSE4 | 1 | 1 |
| NSE5 | 3 | 1 |

**2.5. Drug Solubility.** PTL was dissolved in phosphate buffer pH 7.4 and agitated for 24 h at 200 rpm at 25 °C to test its solubility in free form and in disulfide bridged nanoparticles with PTL loaded on them. The samples were placed for 40 min at 14000 rpm in a centrifuge. PTL concentration was calculated at 240 nm using a UV−vis spectrophotometer after the supernatant was removed. (Analytical curve of PTX standard in phosphate buffer at pH 7.4, range 5−90 $\mu$g/mL, $y = 0.0103x - 0.0129$, $R^2 = 0.9995$).

**2.6. Determination of Thiol Contents.** Using Ellman's reagent and spectrophotometry, the thiol contents of TSA, TERS100, and disulfide bridged nanoparticles (NSE1 to NSE5) were calculated. 500 mL of both thiolated polymers and Ellman's reagent should be mixed in a 1:1 ratio before being dissolved in 1% acetic acid. We separately dissolved TSA, TERS100, and the nanoparticle in phosphate buffer at a pH of 7.4. After 10 min of incubation, measure the absorbance at 412 nm with a UV−visible spectrophotometer for all reaction mixtures.

**2.7. Loading and Entrapment of PTL.** We dispersed 0.01 g of developed nanoparticles in 4 mL of distilled water, and 0.01 g of PTL was added. The mixture was mixed for 24 h before the PTL-loaded nanoparticles were separated by centrifugation at 10,000 rpm. This mixture's supernatant was taken in order to ensure the effectiveness of medication loading. Drug loading was carried out three times in triplicate. Through the use of high performance liquid chromatography (HPLC), the amount of PTL in the supernatant solution was calculated.



https://doi.org/10.1021/acsomega.3c00400
ACS Omega 2023, 8, 9662−9672

$$\%\text{Entrapment efficiency} = \frac{\text{Amount of PTL loaded in nanoparticles}}{\text{Total amount of PTL loaded initially}} \times 100 \quad (2)$$

**2.8. Release of Paclitaxel from Nanoparticles.** Phosphate buffer (pH 7.4) was used to check release of PTL from synthesized nanoparticles of the formulations, and the paddle Apparatus (Pharma-test Germany) was used to compare the PTL release in the presence and absence of GSH. A basket containing 900 mL of dissolution media was filled with 50 mg of nanoparticles and 5 mL of phosphate buffer (pH 7.4) in a dialyzing membrane and held at a temperature of 37 ± 0.5 °C for 24 h. To keep the sink condition in working order, the same buffer of pH 7.4 was replenished, while the 5 mL sample was taken out at defined intervals and filtered via a 0.2 μm filter and analyzed by HPLC for PTL analysis.

**2.9. Release Kinetics.** Mathematical models (zero-order (eq 3), first-order (eq 4), Higuchi (eq 5), Hixon Crowell (eq 6) and Korsmeyer Peppas model (eq 7)) for the approximation of kinetics of PTL from the NSE1 to NSE5 formulations were used.

$$F_t = K_0 t \quad (3)$$

$$\ln(1 - F) = K_1 t \quad (4)$$

$$F = K_2 t^{1/2} \quad (5)$$

$$W_0^{1/3} - W_t^{1/3} = kt \quad (6)$$

$$\frac{M_t}{M_\infty} = K_3 t^n \quad (7)$$

In eqs 3−7, $F_t$ is the fraction of PTL released at time $t$, $K_0$ is the rate constant for zero order, $F$ is fraction of PTL released, $K_1$ is rate constant for first order, $K_2$ is the Higuchi constant, $W_0$ is the initial amount of PTL in nanoparticles, $W_1$ is the remaining amount of PTL in the nanoparticles, $k$ is the rate constant incorporating the surface volume ratio, $M_t$ and $M_\infty$ is the amount of drug released at $t$ and infinity, respectively, and $n$ is the diffusion constant.

**2.10. Characterization.** The $^1$H NMR of the SA, TSA, ERS100, and TERS100 solutions was performed using $^1$H NMR spectroscopy (Bruker Alpha, Germany). The quantity of sample was 20 μg/mL, and the calibration spectra were created at chemical shift ($\delta$). The data were analyzed using the software Mes Res Nova 14.1.0. FTIR spectra of PLT, SA, TSA, ERS100, TERS100, NSE4 (blank), and NSE4 (PTL loaded) nanoparticles were recorded at 400−4000 cm$^{-1}$ using the FTIR spectrophotometer Bruker Alpha, Germany. XRD of PLT, SA, TSA, ERS100, TERS100, and unloaded and PTL loaded nanoparticles were performed using diffractometer. For DCS and TGA analysis, 5 ± 0.5 mg samples of PLT, SA, TSA, ERS100, TERS100, and unloaded and PTL loaded nanoparticles were kept in aluminum crucibles, heated at a temperature range of 50−600 °C with a rate of 10 °C/min, and pass through a stream flow of nitrogen gas at 40 mL/min using DSC (Shimadzu, Germany). Malvern Zeta Sizer (Nano Series ZS90) estimated the particle's size and zeta potential. The homogeneity at a temperature of 25 °C is reflected by the polydispersity index of particle diameter. Three times each measurement was recorded. For a month, these nanoparticles were maintained at pH 7.4 and 25 °C. To ensure the stability, these nanoparticle measurements were made before and after a month. The SEM, JEOL 6700 F was used for the estimation of the NSE4 PTL loaded nanoparticles morphology.

**2.11. Biological Studies.** *2.11.1. Cell Viability Assay.* Cell viability was done by 3-(4,5-dimethylthiazol-2-yl)-2,5- diphenyltetrazolium bromide (MTT) assay.[10] Briefly, Caco-2 cells were seeded up to 90% confluence into 96-well plates in Dulbecco's modified Eagle's medium (DMEM) with 10% fetal bovine serum (FBS). After that, the cells were incubated with 0.5% dispersions of SA, TSA, ERS100, TERS100, NSE4 blank, and PTL-loaded nanoparticles for 6 and 24 h in a medium without FBS. After incubation, the samples were removed and carefully washed three times with phosphate-buffered saline (1×, pH 7.4). After that, each well received 500 μL of medium containing MTT (1 mg/mL final concentration) and was incubated for an additional hour at 37 °C. The transformed dye was solubilizing with 500 μL of dimethyl sulfoxide (DMSO) after the supernatants were removed. The optical density was detected at 570 nm using a microplate reader (Thermo Fisher Scientific, Inc.). Equation 8 was used to measure the % age of cell viability:

$$\text{Cell viability}(\%) = \frac{\text{Absorbance of sample dispersion}}{\text{Absorbance of DMEM dispersion}} \times 100 \quad (8)$$

*2.11.2. Hemolysis Test.* The impact of the NSE4 PTL loaded nanoparticles on rabbit red blood cells (RBCs) were evaluated by the standard hemolysis assays.[11] In a total amount of 5 mL, 2.5 mL of the RBC suspension and different concentrations of the NSE4 nanoparticles were combined. Saline solution was added to the negative control group, whereas deionized water was added to the positive control group. All the above suspensions were incubated at 37 °C for 1 h. In order to remove intact RBCs, all suspensions were centrifuged for 10 min at 3000 rpm. A UV-2450 spectrophotometer (Shimadzu) was used to analyze the collected supernatant for the release of hemoglobin at 541 nm. The hemolysis (%) was estimated using eq 9:

$$\text{Hemolysis}(\%) = \frac{\text{Abs} - \text{Abs}_0}{\text{Abs}_{100} - \text{Abs}_0} \times 100 \quad (9)$$

where Abs, $\text{Abs}_{100}$, and $\text{Abs}_0$ are the samples absorbance, 100% hemolysis solutions, and 0% hemolysis solutions, respectively. By utilizing a sample solution devoid of RBCs as a blank control, the turbidity of the samples was countered.

*2.11.3. Intestinal Permeability Study.* The *in situ* intestinal-perfusion process was employed to measure the intestinal absorption of PTL-loaded nanoparticles.[12] Rats were starved for 12 h before the studies but had free access to water. The abdominal cavity was opened, and a small intestinal portion was exposed with saline solution. Its contents were removed using a flow-pump after a 20% (w/v) urethane injection at a dose of 1 g/kg was given. A pledget covered in saline solution was utilized to surround the surgical area, and a heating light was employed to maintain the rat's normal body temperature. Krebs-buffer Ringer's (KRB) was pumped through the piece of intestine for 10 min with a flow rate of 0.2 mL/min. The drug perfusion solution was then infused at a flow rate of 0.2 mL/min, and the time was set to 0 just as the perfusion started. The perfusion solution contained 30 μg/mL PTL with 20 μg/mL phenol red for each tested sample in KRB. The length of each segment of the intestine was measured together with the


https://doi.org/10.1021/acsomega.3c00400
ACS Omega 2023, 8, 9662−9672

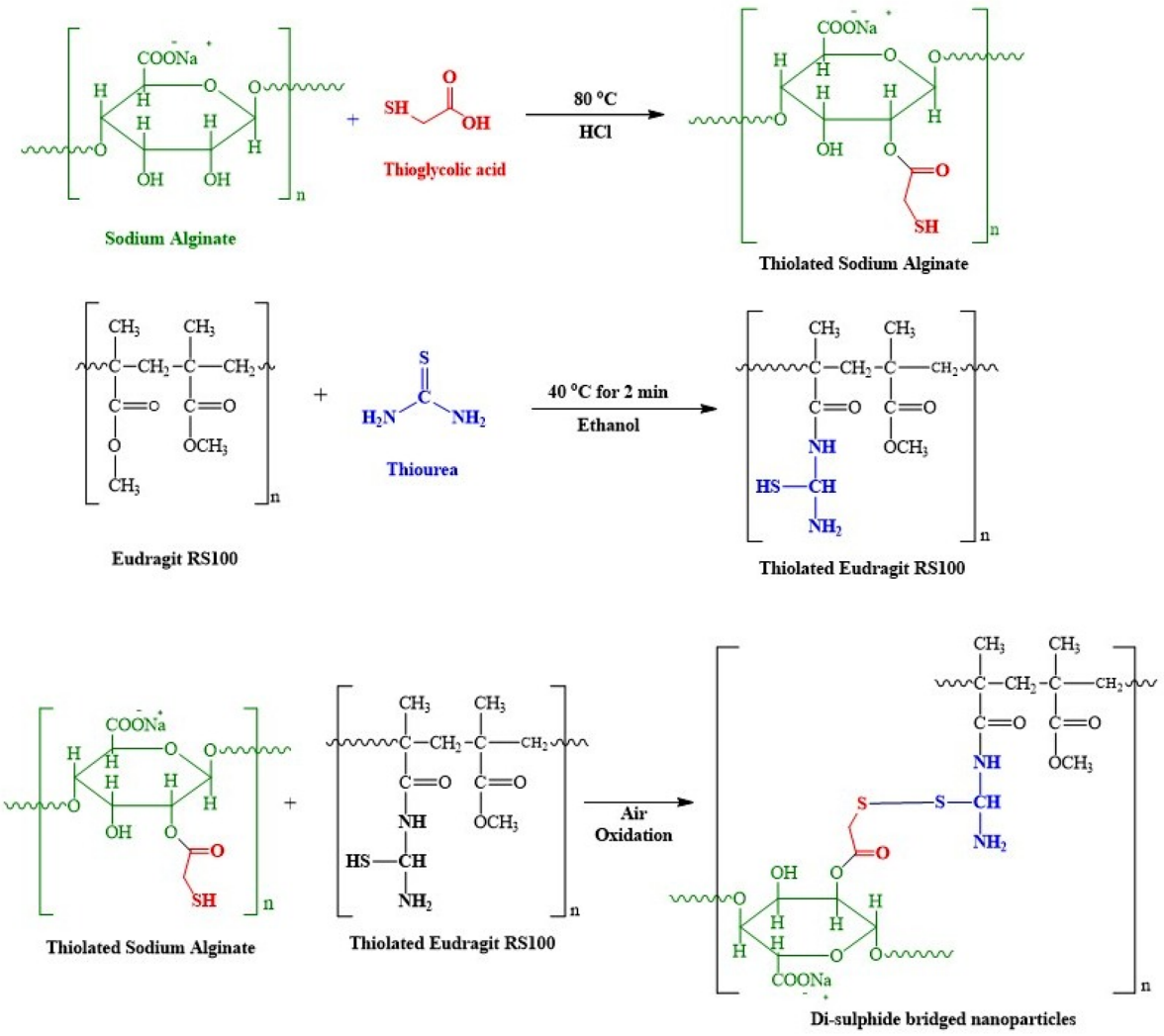


**Figure 1.** Chemical scheme for the thiolation of SA and ERS100 and formation of disulfide bridged nanoparticles.

perfused samples, which were collected every 15 min up to 120 min after steady-state was reached. We next combined 0.8 mL of methanol with 0.2 mL of perfusate, centrifuged at 10,000 rpm for 10 min, and analyzed the supernatant by HPLC for PTL. A UV spectrophotometer was used to quantify the concentration of phenol red at 558 nm with a mixture of 0.1 mL of perfusate and 0.9 mL of NaOH (0.1 M) and effective permeability was determined using eq 10. In eq 10, $Q$ is flow rate of perfusate (0.2 mL/min), $r$ is radius of intestine (0.17 cm), $L$ is intestinal segment length in cm, $C_{in}$ and $C_{out}$ are in-let and out-let perfusate concentration of PTL respectively, and $PR_{in}$ and $PR_{out}$ are the in-let and out-let phenol red concentrations, respectively.

$$\text{Effective permeability} = -\frac{Q}{2\pi rL} In\left(\frac{C_{out}}{C_{in}} \times \frac{PR_{in}}{PR_{out}}\right) \quad (10)$$

*2.11.4. Quantitative Real-Time Polymerase Chain Reaction (qRT-PCR).* qRT-PCR was done for determining the expressionof genes such as E-cadherin, Slug, Twist and $\alpha$-SMA. Total RNA was extracted from cultured cells by TRIzol method and quantified via NanoDrop spectrophotometer measuring absorbance at 260 and 280 nm. RNA samples were transcribed to cDNA using the Thermo Scientific cDNA kit. Glyceraldehyde-3-phosphate dehydrogenase (GADPH) was used as a house keeping gene. Primers (E-cadherin, Slug, Twist, $\alpha$-SMA and GADPH) were designed via use of Gene Bank and primerblast (Table S1). The qRT-PCR was subjected to 40 cycles of thermal cycling, each consisting of denaturation at 95 °C for 15 s, annealing at 60 °C for 20 s, and extension at 72 °C for 20 s. qRT-PCR was used to determine the mRNA expression levels of the genes using Mesa Blue qPCR Master Mix Plus for SYBR assay (Eurogentec) and the Master cycler Realplex2 (Eppendorf). The quantity of the enhanced PCR product in relation to the reference gene (GAPDH) was calculated using cycle threshold (Ct) values.

*2.11.5. Pharmacokinetic Study.* To evaluate the pharmacokinetics of PTL-loaded nanoparticles, 12 albino rats (250−450 g) were split into two groups. The Government College University Faisalabad's ethical committee granted permission for the study, and the ICH rules were followed. On the first day, the rats fasted for 24 h. Rats in group 1 and 2 received 10 mg/kg of the NSE4 formulation (test) and PTL suspension (reference) respectively. The rats' tail vein was used to collect 0.25 mL of blood at predetermined intervals (0, 1, 2, 4, 6, 8, 10, 12, 24, 36, and 48 h). These blood samples were centrifuged at 4500 rpm for 15 min. The plasma was separated, and then deproteinizer was added. It was then subjected to centrifugation for 15 min at 4500 rpm. The supernatant was


https://doi.org/10.1021/acsomega.3c00400
ACS Omega 2023, 8, 9662−9672

remove, filtered through 0.22 $\mu$m filter and injected into HPLC for analysis. $T_{max}$, $C_{max}$, AUMC, MRTm and AUC were estimated employing Kinetica-R-version 4.1.1 by Thermo-Electron Corporation, USA.

**2.12. Statistical Analysis.** SPSS version 17 (SPSS Inc., Chicago, IL, USA) was used to examine the pharmacokinetics data. The parameters between the control and test groups were calculated using the Student's $t$ test, with a 95% confidence interval.

## 3. RESULTS AND DISCUSSION

**3.1. Thiolation of Polymers and Preparation of Nanoparticles.** The nanoparticles (NSE1 to NSE5 formulations) were effectively produced utilizing the air-oxidation method. Figure 1 shows the chemical formula for the design of nanoparticles using TERS100 and TSA. TSA and TERS100 contained 0.17 and 0.13 mmol/mg free thiol groups respectively. Free thiol levels of 0.05−0.13 mmoL/mg were found in nanoparticles. Ho et al. in 2010 studied the similar contents of thiol in the thiolated polymers.[13]

**3.2. Solubility and *In Vitro* Release of PTL.** The water solubility of free PTL and PTL-loaded nanoparticles was determined. PTL had extremely low water solubility (~4.5 $\mu$g/mL). It is interesting to note that PTL-loaded nanoparticles boosted the solubility of PTL by over 11 times (~59 $\mu$g/mL).[14] NSE4 formulation demonstrated 75.34% and 89.18% entrapment and loading efficiency of PTL, respectively. The TSA, TERS100, and PTL ratio in the formulation had an impact on the effectiveness of drug loading and entrapment. Due to the formulation's equal quantity of polymer, entrapment efficiency was increased. The release of PTL was assessed with and without the GSH, because in a malignant situation, the gut formed a reductive environment. As shown in Figure 2, the PTL release from NSE1 to NSE5 ranged from 69.18% to 95.39% when GSH was present, whereas this release ranged from 34.89% to 45.43% when GSH was not present. In cancerous cell, the level of GSH is 7−10 times more than the normal cells. In the presence of GSH, the disulfide bridged nanoparticles are degraded and release of PTL in a controlled mode.[6] These results are comparable with the results of Abouelmagd et al. in 2015.[14] These findings suggested that the release of PTL depends on the reductive environment created by cancer in the colon. In either the presence or absence of GSH, Iqbal et al. investigated the moxifloxacin release from developed formulations of nanoparticles.[9] In zero-order kinetics, $R^2$ values were 0.991−0.997, and $R^2$ in first-order kinetics ranged from 0.823 to 0.918. The formulations, according to the results, followed zero-order kinetics. The Higuchi model's $R^2$ value ranged from 0.995 to 0.999, indicating that diffusion was responsible for the release of PTL from nanoparticles. The fact that the value of $n$ in the Korsmeyer Peppas model was <0.5 suggested that the release of PTL from nanoparticles was fickian-diffusion. The similar findings for the release kinetics of PTL was observed by Hasanbegloo et al. from the developed nanoformulations.[15]

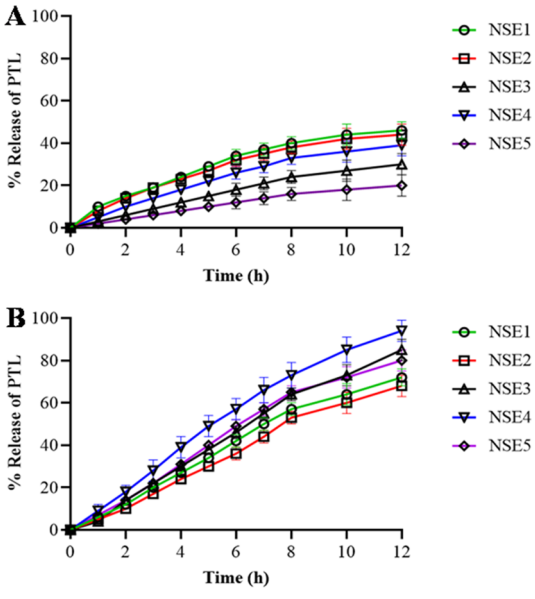


**Figure 2.** Evaluation of *in vitro* release profile of PTL from disulfide bridged nanoparticles in phosphate buffer ph 7.4 in the absence (A) and presence (B) of GSH ($n$ = 6).

**3.3. Characterization.** *3.3.1. $^1$H NMR.* The alkene protons were shown in the range of 3.5−4.5 in the $^1$H NMR spectra of SA, which displayed proton peaks at 3.79, 4.1, and 4.4 ppm contributed to the H of alginate (Figure 3A). On thiolation with TGA, the interaction between the hydrogen atom of SA and the −OH group of TGA causes the proton to exhibit signals at 2.54 ppm, demonstrating that the SA has been efficiently thiolated as shown in the $^1$H NMR spectra of TSA (Figure 3B). Khalid et al. in 2020 studied the similar behavior of thiolation of SA with TGA.[8] $^1$H NMR of ERS100 exhibited peaks at 3.69 and 4.98 ppm correlates to the H of aromatic C−H group (Figure 3C) and 3.24−3.15 and 7.1 ppm peaks were observed in TERS100[9] as shown in Figure 3D. There was a nucleophilic substitution reaction between ERS100 and thiourea. This reaction replaced ester linkage with amide formation.

*3.3.2. Fourier Transforms Infrared Spectroscopy (FTIR).* FTIR spectra of PTL showed characteristic peaks at 3452, 2935, and 2277 cm$^{-1}$ due to −OH bond, alkane −CH, and −C═O vibrations, respectively,[16] as shown in Figure 4A. In SA, the −OH stretching of carboxylic groups was observed at 3123 cm$^{-1}$.[17] Carboxylate anions showed symmetric and asymmetric stretching vibration peaks at 1587 and 1452 cm$^{-1}$, respectively. The adsorption bands of cyclic CH bending and COC cyclic ether stretching were found at 815 and 1022 cm$^{-1}$, respectively. The successful thiolation of SA through ester bonding between carboxyl and hydroxyl group of TGA and SA, respectively, was evidenced by a peak of the thiol group in TSA that was seen at 2279 cm$^{-1}$.[18] Due to −C═O stretching and CH aliphatic stretching, ERS100 had peaks at 1737 and 2937 cm$^{-1}$, respectively,[19] as shown in Figure 4A. The presence of a thiol group at 2553 cm$^{-1}$ in TERS100 validates the thiolation.[9] The ester linkage of ERS100 was replaced with amide group of thiourea during the process of thiolation. FTIR spectra of NSE4 blank nanoparticles showed peak at 1611 cm$^{-1}$ which confirms the formation of disulfide bond (−S−S−) between TSA and TERS100. The PLT loaded NSE4 formulation showed characteristic band peaks of PTL, TSA, and TERS100 polymeric materials and disulfide bond (1611 cm$^{-1}$) indicated the successful entrapment of PTL in the nanoparticles. There were no significant chemical interactions between the PTL and the thiolated polymers utilized in the formulation, as evidenced by the retention of all pure drug peaks in the formulation's FTIR spectrum.


https://doi.org/10.1021/acsomega.3c00400
ACS Omega 2023, 8, 9662−9672

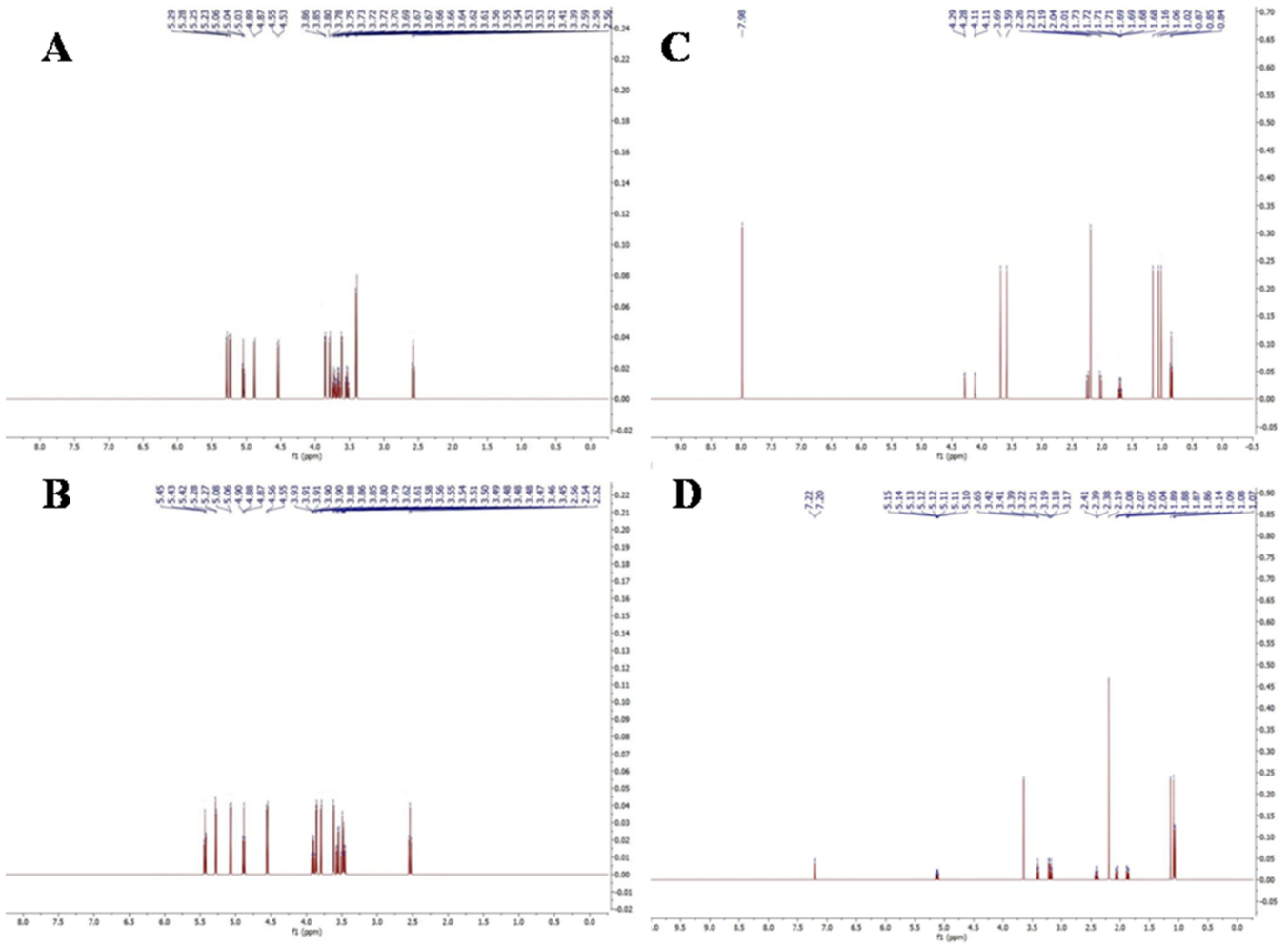


**Figure 3.** $^{1}$H NMR spectra of the sodium alginate (A), thiolated sodium alginate (B), eudragit RS100 (C), and thiolated eudragit RS100 (D).

*3.3.3. X-ray Diffraction (XRD).* PTL had crystalline behavior, exhibiting diffraction peaks at 2$\theta$ of 1°, 7°, 10°, and 15° as well as numerous peaks between 14° and 31°.[20] SA showed many characteristics peaks of diffraction at 2Θ of 10°, 15°, and 16° indicated the presence of hydrogen binding and polar inter- and intramolecular interactions[21] as shown in Figure 4B. The XRD diffractogram of TSA showed peaks at 2Θ of 15°, 16°, 31°, and 32° which confirm the more crystalline nature of TSA. The change in the peaks of TSA suggested that thiol groups bound to SA, altering crystallinity and causing changes in the atomic density of the polymers at the molecular level. ERS110 showed two peaks at 12° and 19°,[22] and the TERS100 showed peaks but the intensity of peaks were low confirmed the process of thiolation. NSE4 blank nanoparticles displayed several peaks, but their low intensity revealed that the particles were amorphous. The absence of PTL peaks in the NSE4 formulation indicates that the drug's crystalline shape was successfully changed to an amorphous form, increasing its solubility and bioavailability.

*3.3.4. Differential Scanning Calorimetry (DSC).* The DSC curves of PTL, SA, TSA, ERS100, TERS100, and nanoparticles of NSE4 (blank) and NSE4 (PTL loaded) are shown in Figure 5A. The PTL showed one endothermic peak at 233.50 °C and second exothermic peak at 247.50 °C indicated the crystalline nature of drug.[23] An endothermic peak of SA was observed at 100 °C may be caused by the loss of moisture and water content. The SA showed exothermic peak at 255.63 °C,[24] and TSA showed an endothermic peak at 220 °C and an exothermic peak 243.75 °C, confirming the process of thiolation.[23] Kassem et al. investigated the DSC thermograms of SA and TSA and found that the heat of fusion of SA decreased following thiolation.[18] The ERS100 showed an endothermic peak at 409.54 °C,[25] and TERS100 showed two endothermic peaks at 76.34 and 379.38 °C as shown in Figure 5. A decrease in the endotherm of TESR100 confirms the thiolation of ERS100.[6] NSE4 blank nanoparticles showed exothermic and endothermic peaks at 354.58 and 377.30 °C respectively. The breakdown of the polymeric components may have caused the exothermic peak to arise in NSE4 blank nanoparticles. Previous research has shown that the degradation of the polymeric materials of nanoparticles to develop exothermic peaks at temperatures higher than 200 °C.[26] The thermogram of NSE4 (PTL-loaded) demonstrates unequivocally that PTL and other used polymers lack their typical exothermic and endothermic peak values. The PTL was converted from a crystalline to an amorphous state during manufacture and/or the drug being dispersed in the polymer matrix, the PTL exothermic and endothermic peaks dissipated in the nanoparticles.[27] It verifies PTL's entrapment inside the polymeric conjugate as well as the drug's molecular dispersion in the polymer matrix.



https://doi.org/10.1021/acsomega.3c00400
ACS Omega 2023, 8, 9662−9672

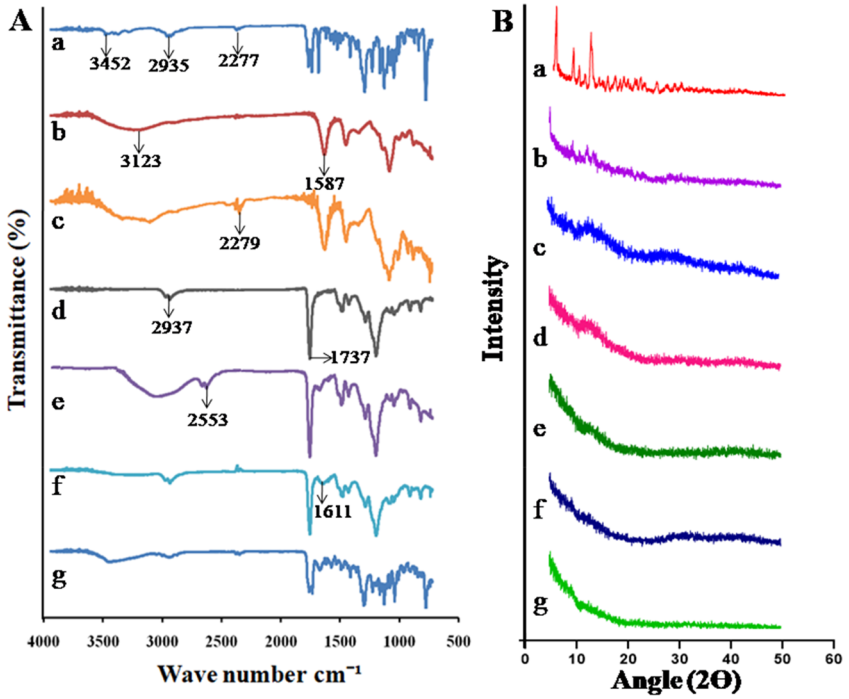


**Figure 4.** FTIR (A) and XRD (B) of PTL (a), SA (b), TSA with thiol group peak at 2279 $cm^{-1}$ (c), ERS100 (d), TERS100 presents peak of thiol group at 2553 $cm^{-1}$ (e), NSE4 blank showed disulfide bond at 1611 $cm^{-1}$ (f), and NSE4 PTL loaded nanoparticles (g).

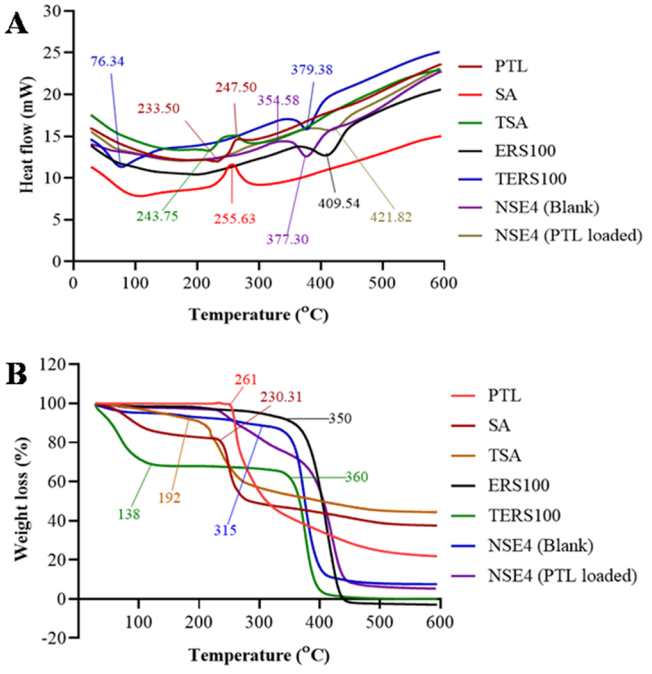


**Figure 5.** DSC (A) and TGA (B) of PTL, SA, TSA showed decrease in endotherm, ERS100, TERS100 presents decrease in endotherm, NSE4 blank, and NSE4 PTL loaded nanoparticles.

*3.3.5. Thermogravimetric Analysis (TGA).* The TGA curves of PTL, SA, TSA, ERS100, TERS100, and nanoparticles of NSE4 (blank) and NSE4 (PTL loaded) are shown in Figure 5B. The weight loss of PTL was started at 261 °C and continued until 600 °C. The free and interlayer water in PTL were lost before 200 °C.[28] The sample of PTL showed good thermal stability below 260 °C. The weight loss of SA started at 33 °C, and 18% weight loss was at 230.31 °C, and after 286.10 °C the loss of weight was slow.[29] In case of TSA 8% weight loss was observed at 192 °C, and after that rapid weight loss was observed and continued until 600 °C. The weight loss of TSA was rapid as compared to sodium alginate. The TGA curve of ERS100 showed slow weight loss initially but at 350 °C the rapid weight loss was observed.[30] In TERS100, the curve showed rapid weight loss at 138 °C, and no weight loss was observed until 355 °C and weight loss happened quickly at 360 °C. The NSE4 blank and PTL loaded nanoparticles showed slow weight loss until 315 °C indicated the thermal stability and effective entrapment of PTL in the formulation. Due to their compact size, prepared nanoparticles were able to withstand high temperatures and demonstrated slower weight loss.[31]

*3.3.6. Particle Size Analysis and Zeta Potential.* The stability, drug release, and pharmacokinetics are all directly impacted by the particle size, making it a crucial parameter. According to photon correlation spectroscopy (PCS), the produced nanoparticles' mean particle sizes ranged from 103 to 145 nm, and all of their size distributions were monodispersed (0.034−0.351).[32] The best size of nanoparticles, which was chosen for further analysis, was 103 nm shown by the NSE4 (Figure 6A). As previously reported for the nanoparticles of nebivolol using Eudragit RS100, there were no notable changes between the diameters of nanoparticles generated with varied drug-polymer ratios.[33] The stability of nanoparticles is intimately correlated with the zeta potential. The zeta potential of nanoparticles with values > +30 mV or < −30 mV suggest a high degree of ionization and, consequently, a larger electrostatic repulsion between the nanoparticles. Aggregation can be decreased under these conditions, enhancing the electrical stability of the systems. In this study, the nanoparticles' ZP measurements revealed a significant amount of negative charge (−21 mV) as shown in Figure 6B.



https://doi.org/10.1021/acsomega.3c00400
ACS Omega 2023, 8, 9662−9672

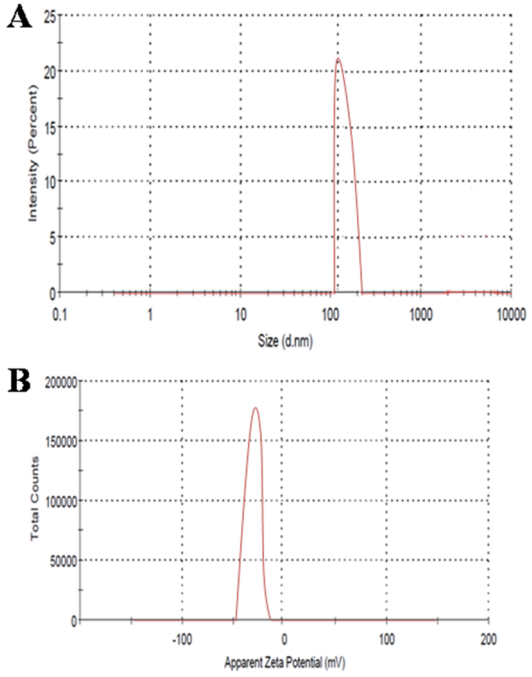


**Figure 6.** Particle size (A) and zeta potential (B) values of NSE4 formulation.

*3.3.7. Scanning Electron Microscopy.* As illustrated in Figure 7, SEM pictures of the PTL-loaded NSE4 formulation

**Figure 7.** SEM image showed rod shape nanoparticles of NSE4 formulation.

revealed rod shape was seen at 200 nm resolutions. The diameter of the nanoparticles ranged from 103 to 200 nm and had a rough surface. The rod-shaped nanoparticles had longer residence duration than the round-shaped particles.[34]

**3.4. Biological Studies.** *3.4.1. Cell Viability, qPCR, and Hemolysis Study.* The inhibition of Caco-2 cells proliferation was observed when these cells were incubated with PTL-loaded nanoparticles of NSE4 as depicted in Figure 8A. Compared to the conventional dose form, our PTL-loaded NSE4 formulation demonstrated a considerable inhibitory effect on EMT in which a significant upregulation of E-cadherin and downregulation of Slug, Twist, and $\alpha$-SMA was observed by qPCR as shown in Figure 8B. This might be due to the cationic surface charge of prepared nanoparticles which improved their cellular penetration due to their electrostatic interaction with the plasma membrane, which has a negative surface charge due to its double-layer phospholipids chains.[11,35] To determine if the nanoparticle formulation was harmful to RBCs, an *in vitro* RBCs lysis test was conducted. Triton X-100 was used as a positive control with 100% RBCs lysis. Compared to the blank formulation of NSE4 nanoparticles, the PTL-loaded nanoparticles induced a very little RBCs lysis suggests that they are suitable for systemic administration[36] (Figure 8C).

*3.4.2. Intestinal Permeability of PTL.* Based on intestinal permeability of PTL in rat intestine segments, the intestinal absorption of NSE4 nanoparticles was assessed. When compared to pure PTL suspension, NSE4's effective permeability of 2.08 cm/s was significantly (2.19-fold) higher than that of 0.95 ± 0.35 cm/s (Figure 8D), indicating that nanoparticles clearly improved intestinal absorption of PTL. Our results of intestinal permeability are comparable to the findings of Qu et al. in 2018 for PTL.[12]

*3.4.3. Pharmacokinetics of PTL.* The pharmacokinetic properties of investigational PTL nanoparticles were determined using the validated HPLC technique. For both pure PTL and PTL loaded nanoparticles (NSE4), a comparison of the mean plasma concentration with time was displayed in Figure 8E. Both profiles displayed the typical biphasic pattern of a phase of fast distribution followed by a phase of elimination. After 12 h, PTL concentration for pure drug was found to be below the HPLC quantification limit, but PTL from NSE4 continued to be detectable for 24 h. The different pharmacokinetic parameters displayed by nanoparticles of NSE4 in contrast to pure PTL are shown in Table 2. In both the distribution phase and the elimination phase, the measured concentrations of PTL supplied as pure drug were substantially lower than those of PTL loaded nanoparticles. Jan et al. in 2002 studied the similar findings of distribution and elimination phase of fluvoxamine.[37] The $AUC_{0-24}$h value of the NSE4 nanoparticles was 4−5 times greater than that of pure PTL. Additionally, PTL half-life ($t_{1/2}$) increased by 3−6 times after exposure to NSE4. These could be the cause of the medicines' reduced clearance as nanoparticles. Zabaleta et al. in 2012 studied the pharmacokinetics of PTL after oral administration and calculated the similar findings of pharmacokinetic values.[38] The amount of plasma elimination rate constant ($K_{el}$) displayed by PTL from NSE4 also indicated that the medications would remain in the body's systemic circulation for a longer period of time. Kamiya et al. in 2018 observed the findings of longer circulation time of drug in rats.[39] The findings demonstrated that the use of nanoparticles of NSE4 successfully eliminated the absorption-related problems associated with PTL. Therefore, PTL loaded nanoparticles may successfully destroy tumor cells with enough retention time, and PTL is thought to have improved anticancer treatment efficacy.

## 4. CONCLUSION

By using the air oxidation approach, disulfide bridged nanoparticles were successfully synthesized, ensuring prolonged delivery of PTL to the target site. In the reductive environment of the colon, this carrier efficiently transported the medications. The created nanoparticles were capable of precise drug release at the target site and efficient targeting. PTL loaded NSE4 nanoparticles induced very minimal RBCs


https://doi.org/10.1021/acsomega.3c00400
ACS Omega 2023, 8, 9662−9672

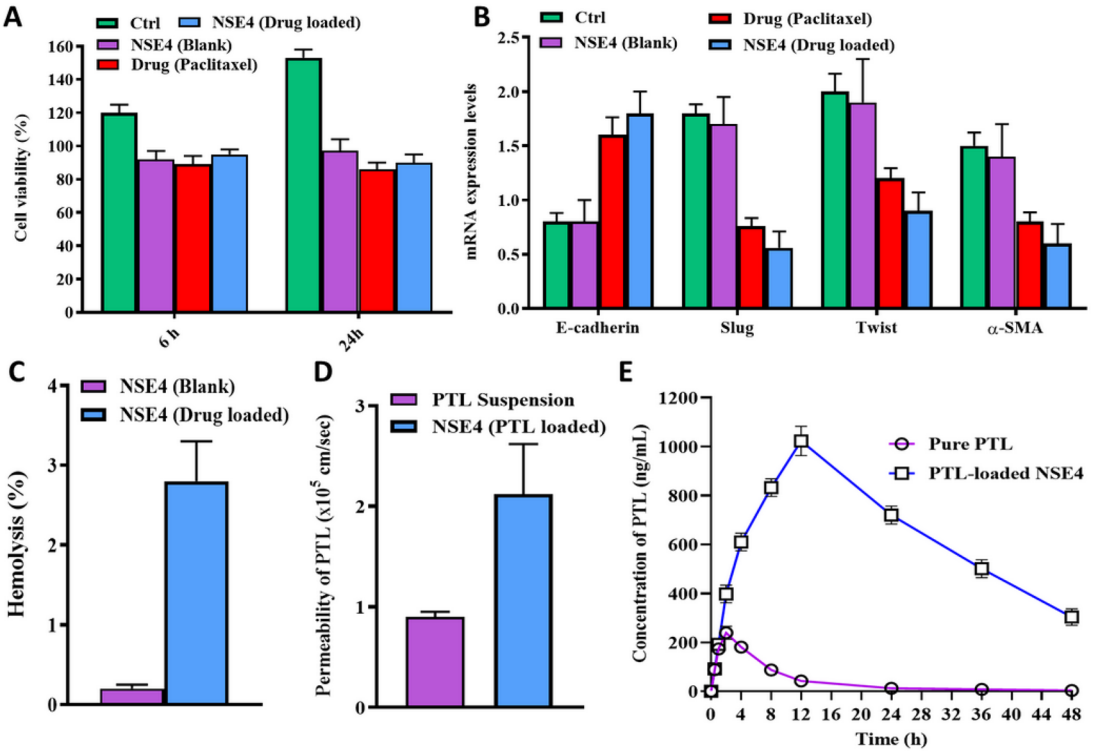


**Figure 8.** Cell proliferation as well as mRNA expression of EMT associated genes, hemolysis, permeability and pharmacokinetic study (A) Cell proliferation is inhibited, and (B) the expression of mesenchymal markers (Slug, Twist and $\alpha$ SMA) were lower, while those of epithelial marker E cadherin was higher in Caco-2 cells following treatment with NSE4 (Drug loaded) as determined by reverse transcription quantitative polymerase chain reaction (C) *in vitro* hemolysis assay for NSE4 (Bland) and NSE4 (Drug loaded) is below 5% (D) the effective permeability of PTL suspension and NSE4 (Drug loaded) in mice intestine and (E) pharmacokinetics of PTL from NSE4 PTL loaded nanoparticles.

**Table 2. Parameters of Pharmacokinetics of Pure PTL and PTL-Loaded NSE4 Nanoparticles**

| parameters | pure PTL | PTL-loaded NSE4 |
|---|---|---|
| $C_{max}$ (ng/mL) | 239 ± 26.234 | 1023 ± 60.786 |
| $T_{max}$ (h) | 2 ± 0.050 | 12 ± 1.023 |
| $AUC_{0-t}$ (ng·h/mL) | 2827 ± 56.786 | 12405 ± 78.876 |
| $AUC_{0-\infty}$ (ng·h/mL) | 2983 ± 53.123 | 13129 ± 87.654 |
| $K_{el}$ | 0.072 ± 0.001 | 0.234 ± 0.031 |
| $t_{1/2}$ (h) | 8.76 ± 1.098 | 40.98 ± 3.910 |

lysis and had a stronger inhibitory effect on EMT. Additionally, the pharmacokinetic characteristics showed that NSE4 had a longer circulatory residence and slower clearance rate compared to control. The NSE4 is a good candidate for therapeutic uses, according to the pharmacokinetic studies. The findings of our study, taken together, may open the door to the logical design of nanoparticles with the appropriate pharmacokinetic properties, capable of improving the *in vivo* efficacy of treatments. The disulfide bridged nanocarrier has the potential to be a promising carrier with clinical uses in the future. Nanocarriers that have been developed could offer a new option for treating CRC with PTL. A novel approach to treating CRC is the PTL medicines in nanoparticulate form.

## ■ ASSOCIATED CONTENT

### Supporting Information

The Supporting Information is available free of charge at https://pubs.acs.org/doi/10.1021/acsomega.3c00400.

$^1$H NMR spectral data for the polymers (sodium alginate, thiolated sodium alginate, eudragit RS100 and thiolated eudragit RS100) and list of primers used in the study (PDF)

## ■ AUTHOR INFORMATION


### Corresponding Authors

**Akhtar Rasul** − *Department of Pharmaceutics, Faculty of Pharmaceutical Sciences, Government College University, Faisalabad 38040, Pakistan*; Phone: 0092419201036; Email: akhtar.rasul@gcuf.edu.pk

**Shahid Shah** − *Department of Pharmacy Practice, Faculty of Pharmaceutical Sciences, Government College University, Faisalabad 38040, Pakistan*; Phone: 0092419201036; Email: shahid.waris555@gmail.com

### Authors

**Hafiz Muhammad Bilal Khalid** − *Department of Pharmaceutics, Faculty of Pharmaceutical Sciences, Government College University, Faisalabad 38040, Pakistan*

**Ghulam Abbas** − *Department of Pharmaceutics, Faculty of Pharmaceutical Sciences, Government College University, Faisalabad 38040, Pakistan*; orcid.org/0000-0002-4531-3911

**Abid Mahmood** − *Department of Pharmaceutical Chemistry, Faculty of Pharmaceutical Sciences, Government College University, Faisalabad 38040, Pakistan*

Complete contact information is available at: https://pubs.acs.org/10.1021/acsomega.3c00400


### Notes

The authors declare no competing financial interest.



https://doi.org/10.1021/acsomega.3c00400
ACS Omega 2023, 8, 9662−9672

## ■ ACKNOWLEDGMENTS

The authors are highly thankful to the Government College University Faisalabad, Pakistan, for providing the research facilities.

## ■ REFERENCES

(1) Deng, L.; Dong, H.; Dong, A.; Zhang, J. A strategy for oral chemotherapy via dual pH-sensitive polyelectrolyte complex nanoparticles to achieve gastric survivability, intestinal permeability, hemodynamic stability and intracellular activity. *Eur. J. Pharm. Biopharm.* **2015**, *97*, 107−117.

(2) Ayub, A. D.; Chiu, H. I.; Mat Yusuf, S. N. A.; Abd Kadir, E.; Ngalim, S. H.; Lim, V. Biocompatible disulphide cross-linked sodium alginate derivative nanoparticles for oral colon-targeted drug delivery. *Artificial cells, nanomedicine, and biotechnology* **2019**, *47* (1), 353−369.

(3) Ding, Y.-F.; Sun, T.; Li, S.; Huang, Q.; Yue, L.; Zhu, L.; Wang, R. Oral colon-targeted konjac glucomannan hydrogel constructed through noncovalent cross-linking by cucurbit [8] uril for ulcerative colitis therapy. *ACS applied bio materials* **2020**, *3* (1), 10−19.

(4) Politi, F. A. S.; Carvalho, S. G.; Rodero, C. F.; Dos Santos, K. P.; Meneguin, A. B.; Sorrechia, R.; Chiavacci, L. A.; Chorilli, M. Piperine-loaded nanoparticles incorporated into hyaluronic acid/sodium alginate-based membranes for the treatment of inflammatory skin diseases. *Int. J. Biol. Macromol.* **2023**, *227*, 736−748.

(5) Rostami, E. Recent achievements in sodium alginate-based nanoparticles for targeted drug delivery. *Polym. Bull.* **2022**, *79* (9), 6885−6904.

(6) Sood, A.; Dev, A.; Mohanbhai, S. J.; Shrimali, N.; Kapasiya, M.; Kushwaha, A. C.; Roy Choudhury, S.; Guchhait, P.; Karmakar, S. Disulfide-bridged chitosan-Eudragit S-100 nanoparticles for colorectal cancer. *ACS Applied Nano Materials* **2019**, *2* (10), 6409−6417.

(7) Raza, F.; Zafar, H.; Khan, M. W.; Ullah, A.; Khan, A. U.; Baseer, A.; Fareed, R.; Sohail, M. Recent advances in the targeted delivery of paclitaxel nanomedicine for cancer therapy. *Materials Advances* **2022**, *3* (5), 2268−2290.

(8) Khalid, S.; Abbas, G.; Hanif, M.; Shah, S.; Shah, S. N. H.; Jalil, A.; Yaqoob, M.; Ameer, N.; Anum, A. Thiolated sodium alginate conjugates for mucoadhesive and controlled release behavior of metformin microspheres. *Int. J. Biol. Macromol.* **2020**, *164*, 2691−2700.

(9) Iqbal, O.; Shah, S.; Abbas, G.; Rasul, A.; Hanif, M.; Ashfaq, M.; Afzal, Z. Moxifloxacin loaded nanoparticles of disulfide bridged thiolated chitosan-eudragit RS100 for controlled drug delivery. *Int. J. Biol. Macromol.* **2021**, *182*, 2087−2096.

(10) Kang, T.; Guan, R.; Chen, X.; Song, Y.; Jiang, H.; Zhao, J. In vitro toxicity of different-sized ZnO nanoparticles in Caco-2 cells. *Nanoscale Res. Lett.* **2013**, *8* (1), 496.

(11) Dobrovolskaia, M. A.; Clogston, J. D.; Neun, B. W.; Hall, J. B.; Patri, A. K.; McNeil, S. E. Method for analysis of nanoparticle hemolytic properties in vitro. *Nano Lett.* **2008**, *8* (8), 2180−2187.

(12) Qu, X.; Zou, Y.; He, C.; Zhou, Y.; Jin, Y.; Deng, Y.; Wang, Z.; Li, X.; Zhou, Y.; Liu, Y. Improved intestinal absorption of paclitaxel by mixed micelles self-assembled from vitamin E succinate-based amphiphilic polymers and their transcellular transport mechanism and intracellular trafficking routes. *Drug delivery* **2018**, *25* (1), 210−225.

(13) Ho, Y.-C.; Wu, S.-J.; Mi, F.-L.; Chiu, Y.-L.; Yu, S.-H.; Panda, N.; Sung, H.-W. Thiol-modified chitosan sulfate nanoparticles for protection and release of basic fibroblast growth factor. *Bioconjugate Chem.* **2010**, *21* (1), 28−38.

(14) Abouelmagd, S. A.; Sun, B.; Chang, A. C.; Ku, Y. J.; Yeo, Y. Release kinetics study of poorly water-soluble drugs from nanoparticles: are we doing it right? *Mol. Pharmaceutics* **2015**, *12* (3), 997−1003.

(15) Hasanbegloo, K.; Banihashem, S.; Faraji Dizaji, B.; Bybordi, S.; Farrokh-Eslamlou, N.; Abadi, P. G.-s.; Jazi, F. S.; Irani, M. Paclitaxel-loaded liposome-incorporated chitosan (core)/poly (ε-caprolactone)/chitosan (shell) nanofibers for the treatment of breast cancer. *Int. J. Biol. Macromol.* **2023**, *230*, 123380.

(16) Shetty, A.; Nagesh, P. K.; Setua, S.; Hafeez, B. B.; Jaggi, M.; Yallapu, M. M.; Chauhan, S. C. Novel paclitaxel nanoformulation impairs de novo lipid synthesis in pancreatic cancer cells and enhances gemcitabine efficacy. *ACS omega* **2020**, *5* (15), 8982−8991.

(17) Eltaweil, A. S.; Mamdouh, I. M.; Abd El-Monaem, E. M.; El-Subruiti, G. M. Highly efficient removal for methylene blue and Cu2+ onto UiO-66 metal-organic framework/carboxylated graphene oxide-incorporated sodium alginate beads. *ACS omega* **2021**, *6* (36), 23528−23541.

(18) Kassem, A. A.; Farid, R. M.; Issa, D. A. E.; Khalil, D. S.; Abd-El-Razzak, M. Y.; Saudi, H. I.; Eltokhey, H. M.; El-Zamarany, E. A. Development of mucoadhesive microbeads using thiolated sodium alginate for intrapocket delivery of resveratrol. *Int. J. Pharm.* **2015**, *487* (1−2), 305−313.

(19) Bharate, S. S.; Kumar, V.; Singh, G.; Singh, A.; Gupta, M.; Singh, D.; Kumar, A.; Vishwakarma, R. A.; Bharate, S. B. Preclinical development of Crocus sativus-based botanical lead IIIM-141 for Alzheimer's disease: Chemical standardization, efficacy, formulation development, pharmacokinetics, and safety pharmacology. *Acs Omega* **2018**, *3* (8), 9572−9585.

(20) Zhao, B.; Du, J.; Zhang, Y.; Gu, Z.; Li, Z.; Cheng, L.; Li, C.; Hong, Y. Polysaccharide-coated porous starch-based oral carrier for paclitaxel: Adsorption and sustained release in colon. *Carbohydr. Polym.* **2022**, *291*, 119571.

(21) Li, Q.-Q.; Wang, Y.-S.; Chen, H.-H.; Liu, S.; Li, M. Retardant effect of sodium alginate on the retrogradation properties of normal cornstarch and anti-retrogradation mechanism. *Food Hydrocolloids* **2017**, *69*, 1−9.

(22) Trapani, A.; Laquintana, V.; Denora, N.; Lopedota, A.; Cutrignelli, A.; Franco, M.; Trapani, G.; Liso, G. Eudragit RS 100 microparticles containing 2-hydroxypropyl-β-cyclodextrin and glutathione: Physicochemical characterization, drug release and transport studies. *European journal of pharmaceutical sciences* **2007**, *30* (1), 64−74.

(23) Zhao, L.; Feng, S.-S.; Kocherginsky, N.; Kostetski, I. DSC and EPR investigations on effects of cholesterol component on molecular interactions between paclitaxel and phospholipid within lipid bilayer membrane. *International journal of pharmaceutics* **2007**, *338* (1−2), 258−266.

(24) Askarzadeh, N.; Nazarpak, M. H.; Mansoori, K.; Farokhi, M.; Gholami, M.; Mohammadi, J.; Mottaghitalab, F. Bilayer Cylindrical Conduit Consisting of Electrospun Polycaprolactone Nanofibers and DSC Cross-Linked Sodium Alginate Hydrogel to Bridge Peripheral Nerve Gaps. *Macromol. Biosci.* **2020**, *20* (9), 2000149.

(25) Lin, S.-Y.; Cheng, W.-T.; Wei, Y.-S.; Lin, H.-L. DSC-FTIR microspectroscopy used to investigate the heat-induced intramolecular cyclic anhydride formation between Eudragit E and PVA copolymer. *Polym. J.* **2011**, *43* (6), 577−580.

(26) Eltayb, E. K.; Aleanizy, F. S.; Alqahtani, F. Y.; Alkahtani, H. M.; Ansari, S. A.; Alsarra, I. Preparation and characterization of Meta-bromo-thiolactone calcium alginate nanoparticles. *Saudi Pharmaceutical Journal* **2022**, *30* (7), 946−953.

(27) Mohammadi, G.; Namadi, E.; Mikaeili, A.; Mohammadi, P.; Adibkia, K. Preparation, physicochemical characterization and antifungal evaluation of the Nystatin-loaded Eudragit RS100/PLGA nanoparticles. *Journal of Drug Delivery Science and Technology* **2017**, *38*, 90−96.

(28) Gibson, J. D.; Khanal, B. P.; Zubarev, E. R. Paclitaxel-functionalized gold nanoparticles. *J. Am. Chem. Soc.* **2007**, *129* (37), 11653−11661.

(29) Sood, A.; Arora, V.; Shah, J.; Kotnala, R.; Jain, T. K. Multifunctional gold coated iron oxide core-shell nanoparticles stabilized using thiolated sodium alginate for biomedical applications. *Materials Science and Engineering: C* **2017**, *80*, 274−281.

(30) Joshi, M.; Sharma, V.; Pathak, K. Matrix based system of isotretinoin as nail lacquer to enhance transungal delivery across human nail plate. *Int. J. Pharm.* **2015**, *478* (1), 268−277.



https://doi.org/10.1021/acsomega.3c00400
ACS Omega 2023, 8, 9662−9672

(31) (a) Li, W.; Li, W.; Wan, Y.; Wang, L.; Zhou, T. Preparation, characterization and releasing property of antibacterial nano-capsules composed of ε-PL-EGCG and sodium alginate-chitosan. *Int. J. Biol. Macromol.* **2022**, *204*, 652−660. (b) Baig, M. M. F. A.; Naveed, M.; Abbas, M.; Kassim, S. A.; Sohail, M.; Ullah, S.; Younis, M. R.; Nawaz, W.; Khan, G. J.; Ansari, M. T. Evaluation of chitosan/eudragit hybrid coating over cubic DNA nanospheres with superior stability and therapeutic outcomes. *Journal of Drug Delivery Science and Technology* **2019**, *52*, 577−585.
(32) Akbari, B.; Tavandashti, M. P.; Zandrahimi, M. Particle size characterization of nanoparticles-a practicalapproach. *Iran. J. Mater. Sci. Eng.* **2011**, *8* (2), 48−56.
(33) Jana, U.; Mohanty, A. K.; Manna, P. K.; Mohanta, G. P. Preparation and characterization of nebivolol nanoparticles using Eudragit RS100. *Colloids Surf., B* **2014**, *113*, 269−275.
(34) Ma, L.; Kohli, M.; Smith, A. Nanoparticles for combination drug therapy. *ACS Nano* **2013**, *7* (11), 9518−9525.
(35) Huang, B.; Tan, Z.; Bohinc, K.; Zhang, S. Interaction between nanoparticles and charged phospholipid membranes. *Phys. Chem. Chem. Phys.* **2018**, *20* (46), 29249−29263.
(36) Burlui, V.; Popa, M.; Cadinoiu, A. N.; Stadoleanu, C.; Mihalache, G.; Zamaru, V.; Dârţu, L.; Folescu, E.; Raţă, D. M. Physico-Chemical Characterization and in Vitro Hemolysis Evaluation of Titanium Dioxide Nanoparticles. *Int. J. Med. Dentistry* **2015**, *5*.87162
(37) Jann, M. W.; ZumBrunnen, T. L.; Kazmi, Y. R.; VanDenBerg, C. M.; Desai, H. D.; Weidler, D. J.; Flockhart, D. A. Pharmacokinetics of fluvoxamine in relation to CYP2C19 phenotype and genotype. *Drug metabolism and drug interactions* **2002**, *19* (1), 1−12.
(38) Zabaleta, V.; Ponchel, G.; Salman, H.; Agüeros, M.; Vauthier, C.; Irache, J. M. Oral administration of paclitaxel with pegylated poly (anhydride) nanoparticles: permeability and pharmacokinetic study. *Eur. J. Pharm. Biopharm.* **2012**, *81* (3), 514−523.
(39) Kamiya, Y.; Otsuka, S.; Miura, T.; Takaku, H.; Yamada, R.; Nakazato, M.; Nakamura, H.; Mizuno, S.; Shono, F.; Funatsu, K.; et al. Plasma and hepatic concentrations of chemicals after virtual oral administrations extrapolated using rat plasma data and simple physiologically based pharmacokinetic models. *Chemical research in toxicology* **2019**, *32* (1), 211−218.


https://doi.org/10.1021/acsomega.3c00400
*ACS Omega* 2023, 8, 9662−9672